Colorimetric Indicator Based on Gold Nanoparticles and Sodium Alginate for Monitoring Fish Spoilage

Lissage Pierre *, Julio Bruna *, Patricio Leyton Bongiorno, Francisco Rodríguez-Mercado, Alejandra Torres

Posted Date: 19 December 2023

doi: 10.20944/preprints202312.1410.v1

Keywords: gold nanoparticles; polymer; colorimetric indicator; sodium alginate; biogenic amines; ethylenediamine

Article

Colorimetric Indicator Based on Gold Nanoparticles and Sodium Alginate for Monitoring Fish Spoilage

Lissage Pierre [1,2,3,*], Julio. E. Bruna [1,2,3], Patricio Leyton [4], Francisco Rodríguez Mercado [1,2,3] and Alejandra Torres [1,2,3]

[1] University of Santiago of Chile (USACH), Packaging Innovation Center (LABEN), Santiago, Chile
[2] University of Santiago of Chile (USACH), Center for the Development of Nanoscience and Nanotechnology (CEDENNA), Santiago, Chile
[3] University of Santiago of Chile (USACH), Technological Faculty, Food Science and Technology Department (DECYTAL), Ave. Víctor Jara 3769, 9170124 Santiago, Chile
[4] Pontificia Universidad Católica de Valparaíso, Instituto de Química, Valparaíso 46383, Chile
* Correspondence: author: lissage.pierre@usach.cl; Tel: +56-937564320. Julio.bruna@usach.cl

Abstract: In this work, a colorimetric indicator based on gold nanoparticles (AuNP) and a biodegradable and eco-friendly polymer (sodium alginate, Alg.), has been developed, for the real-time detection of fish spoilage products. AuNP and colorimetric indicator were characterized by: UV-Vis, FTIR spectroscopies, TGA, DSC, XRD, TEM, and colorimetry. The UV-Vis spectrum and TEM showed the successful synthesis, the spherical shape, and the size of AuNPs. Results indicated color changes of the indicator in packaged fish on day 9 of storage at refrigerated temperature (5ºC). These results showed the successful application of colorimetric indicator in the detection of TVB-N in packaged fish.

Keywords: gold nanoparticles; polymer; colorimetric indicator; sodium alginate; biogenic amines; ethylenediamine

1. Introduction

Fish is an excellent source of nutrients and is easily digestible for the human diet [1] because it contains healthy fats, omega-3 (EPA, DHA), high-quality protein, iron, phosphorus, zinc and selenium, vitamins, and minerals. However, it is highly perishable, vulnerable, and is very prone to spoilage by enzymatic reaction or microbial contamination during handling, distribution, and/or storage due to postmortem modifications followed by the formation of organic acids, aldehydes, ketones, alcohols and sulfides. Improper storage of fish and/or temperature abuse can lead to the formation of Biogenic Amines (BA) [2], among which the most abundant are putrescine, cadaverine, tyramine, and histamine, some of which are harmful to the human organism [3]. In the same way, other factors that play an important role in the deterioration of fish with the consequent production of (BA) are bacteria; mainly gram-positive and negative bacteria. In general, they are located in different parts of the fish body, particularly in the skin, gills, or gastrointestinal tract [4–6], and can also spread in the muscle mass during evisceration through rupture or loss of gastric contents. The species most frequently found in this decomposition process are *Enterobacteriaceae*, including mesophilic and psychrotolerant bacteria, such as *Morganella, Enterobacter*, gram-negative bacteria of the *Hafniaceae* family: *Hafnia, Proteus,* and *Photobacteria* [7]. Furthermore, *Pseudomonas spp*. and lactic acid bacteria belonging to the genera *Lactobacillus* and *Enterococcus* can cause BA formation [8].

In this sense, in recent times various techniques have been used to detect the quality of fish, but it is mainly based on the analysis of its structure (tenderness, color, texture, etc.), using methods of counting bacteria, determining total volatile basic nitrogen (TVB-N) and measuring pH values. Other techniques such as optical spectroscopy, Nuclear Magnetic Resonance (NMR), Fourier-transform infrared spectroscopy (FTIR), and gas chromatography-mass spectrometry (GC/MS) are also used for

 doi:10.20944/preprints202312.1410.v1

evaluation. However, there are disadvantages associated with the use of these techniques, because in some cases the sample is destroyed, a complex, slow, expensive sample preparation is required, and in general an expert person is required to execute the methods [9]. Therefore, the intelligent packaging system is elaborated by the incorporation of a device that can interact internally or externally, monitoring the changes that may occur in the packaged product. This can be divided into three categories: (1) indicators that can provide information to consumers about the quality of food; (2) sensors that are capable of detecting specific analytes in packaged foods; and (3) data carriers (e.g., barcodes and radio frequency identification tags), which are intended for traceability purposes in the food supply chain [10–12].

In this context, sodium alginate is an anionic polymer produced by brown algae and bacteria. It is a biocompatible, biodegradable, non-toxic, low-cost, and readily available polymer. It consists of α-L-guluronic acid (G) and β-D-mannuronic acid (M) residues linked linearly by 1,4-glycosidic bonds [13]. Thus, it is widely used in various fields and in the food industry because it is capable of producing strong gels in the presence of metal cations. Thus, it is considered convenient to develop an indicator based on metallic nanoparticles inserted in the alginate.

In this sense, colorimetric indicators are particularly attractive for on-site applications, because they are relatively simple, inexpensive, and can be read directly with the naked eye [14]. Therefore, in previous studies, researchers have developed a colorimetric label based on bacterial cellulose with the incorporation of grape anthocyanin that allows monitoring the freshness of stored minced meat [15].

Wang et al. [16] reported the development of a simple and elementary colorimetric sensor that can be used as an indicator to detect the freshness of fish using PANI films which are films capable of regenerating by acid solution. He also reported the development of a combined pH and dye-based colorimetric freshness indicator as a "chemical barcode" for real-time monitoring of skinless chicken breast spoilage. Furthermore, Ding et al. [17] developed a polyvinyl alcohol/cellulose-based pH sensor to monitor food quality; after contact with deteriorating shrimp, a color change occurs from yellow to Brown.

On the other hand, other groups of researchers developed an indicator matrix with 16 diverse detection components to monitor fish spoilage [18]. Although the colorimetric indicator based on pH-sensitive dyes is a simple way to control the quality of food, which can be observed with the naked eye. However, it is essential to develop a new detection system based on metal nanoparticles inserted in a biodegradable and eco-friendly polymer for real-time monitoring of fish deterioration. In this research work, a colorimetric indicator based on gold nanoparticles and a natural polymer was developed, capable of indicating, through a color change, when the fish is unsuitable for consumption.

2. Materials and Methods

2.1. Materials

To obtain gold nanoparticles (AuNP), sodium tetrachloroaurate (III) dihydrate ($NaAuCl_4.2H_2O$) 99% CAS No 13874-02-07 and trisodium citrate dihydrate (NaCit) ($C_6H_5Na_3O_7{\cdot}2H_2O$) CAS-No 6132-04-3, were used as reagents and which were purchased from Sigma-Aldrich and used without further purification and distilled water.

2.2. Synthesis and characterization of gold nanoparticles (AuNP)

Gold nanoparticles (AuNPs) were synthesized using the method described by El-Nour et al. [19] with some modifications. Briefly, 40 mL of distilled water were poured into 100-mL flask and heated until boiling, then one milliliter of 1% trisodium citrate was gradually added with continuous stirring. After, 100 µL of 1% sodium tetrachloroaurate (III) dihydrate solution was added and the solution was stirred and heated till the color of the solution changed from yellow to deep red at about 5 min indicating the formation of AuNP. The gold nanoparticles were gradually formed as the citrate

 doi:10.20944/preprints202312.1410.v1

reduces Au^{3+} to Au^{0} as indicated by the red color. AuNP solution was cooled down at room temperature and stored at 4°C until further use.

2.3. Colorimetric indicator preparation

Colorimetric indicators were prepared according to a method described by Dudnik et al. [20]. Briefly, an aqueous solution was added to sodium alginate (2 wt%) and stirred at 1000 rpm for 3h or until complete dissolution. Then, 3 mL of dispersion of gold nanoparticles was added to 1 mL of sodium alginate with continuous stirring. Then, the colloidal suspension was cast into a Petri dish containing 0.10 mol/L solution of calcium chloride to obtain an alginate gel and allowed to dry at ambient conditions. The prepared colorimetric indicators were then packed in a 20 mL screw-cap vial and stored at room temperature until further use.

2.4. Characterization

2.5. UV-VIS spectroscopy

The synthesized AuNP was characterized by the UV-VIS spectrophotometer Spectroquant® pharo 300M, in the range of 300–800 nm. The samples were placed in the cuvette, and the UV-VIS spectrum was measured at different time intervals.

2.6. Fourier transform infrared spectroscopy (FTIR) analysis

FTIR was used to characterize the chemical structure of materials (sodium alginate and gold nanoparticles). For this, a colloidal solution of nanoparticles was concentrated under a vacuum (vacuum system) in a rotary evaporator (Heidolph, Germany) and dried by lyophilization. For analysis, pellets were obtained by mixing, dry gold nanoparticles with KBr 1.0 wt% of the sample. The FTIR equipment model Alpha II Bruker was used at the following conditions: range of 4000–500 cm^{-1}, resolution of 4 cm^{-1} obtained after cumulating 64 scans for determining FTIR of AuNP and indicators respectively.

2.7. Thermal analysis through TGA/DSC analysis

To determine the thermal property of gold nanoparticles (AuNP) and the colorimetric indicator, thermogravimetric analysis was performed on a thermogravimetric analyzer (METTLER TOLEDO Gas Controller GC20 Stare system TGA/DSC) at a rate of 10°C min^{-1} under nitrogen gas flowing at 20 mL min^{-1} in the range of 30–800°C. DSC analyses were carried out on a (DSC1 equipment, model STAR System 822, operating at the following conditions: heating rate of 10 °C min^{-1}, nitrogen flow rate of 20 mL min^{-1}, temperature range from 0 to 400 °C and 0-200°C for AuNP and indicators respectively.

2.8. Detection capacity of gold nanoparticles

The detection capacity of gold nanoparticles was evaluated by preparing a stock solution of ethylenediamine (ETD) with a concentration of 2000 ppm (mg/L) from which the following concentrations 10-400 ppm were obtained.

2.9. TEM

The morphology of the AuNP was studied using Transmission Electron Microscopy (TEM) images (Talos F200X (Thermo Fisher Scientific). The microscope was operated at an accelerating voltage of 200 kV. The sample (10 µL) was mounted on a copper grid covered by a carbon-formvar film and allowed to dry at room temperature for 24 hours before TEM analysis.

 doi:10.20944/preprints202312.1410.v1

2.10. Colorimetry

Colorimetric analysis of AuNP and the colorimetric indicator was performed by obtaining photographs with a digital camera. The photographs obtained were evaluated with the ImageJ software, determining the color parameters (L*, a*, and b*) based on the CIELab color system, and the total color difference according to the following formula:

$$\Delta E = \sqrt{(\Delta L^*)^2 + (\Delta a^*)^2 + (\Delta b^*)^2}$$

L* = lightness (0 = black, 100 = white), + b* (yellow), -b* (blue), + a*(red), -a*(green).

2.11. X-ray diffraction (XRD)

X-ray diffraction (XRD) analysis was carried out using an X-ray diffractometer (D8 Advance, Bruker, Germany) in the range of 2–80° at an angle of 2θ with CuKα radiation, 30 mA, and a scan rate of 6° /min.

2.12. Evaluation of indicators under simulated conditions (In vitro)

The *in vitro* evaluation of the colorimetric indicator was performed with ETD using the method described by Zhai et al. [21]. with slight modifications. For this, the aforementioned indicator was taken and placed in a clean and smooth plastic Petri dish with a 90 mm diameter with ETD solution at room temperature, observing the possible color changes of the indicator. Then, the indicators were peeled from the Petri dishes and were observed in an optical microscope, taking photos with a Samsung smartphone (Galaxy A21S). Then, the total color differences were analyzed with ImageJ software in triplicate and the data was processed in the CIELAB system to determine the color parameters (L*, a*, and b*) [22].

2.13. Evaluation of the indicator in real packaging conditions

2.14. Preparation of packaging for the evaluation of the colorimetric indicator to monitor fish spoilage

For the evaluation of the indicator in real packaging conditions, Atlantic salmon was used as a model food, which was purchased in the local trade. For this, the fish were aseptically filleted with a knife to obtain more or less uniform rectangular samples of equal weight (approximately 50 g). All the fish samples were introduced into a sterile vacuum stomacher bag, in which the colorimetric indicator to be evaluated was inserted, using a polyethylene/polyamine support so that the indicator was kept in direct contact with the muscle food. The stomacher bags were stored at a temperature of 5°C for 9 days to monitor the spoilage and color change of the indicator. At specified intervals during the storage period, the samples were analyzed for any chemical or microbial changes. Reference stomach bags containing fish samples without indicators were also maintained for the same experimental period as those containing indicators.

2.15. Characterization of fish samples during storage

In all fish samples, pH and total volatile basic nitrogen (TVB-N) were determined in duplicate (n=2).

pH measurements were made using a Meat pH Tester (Hanna Instruments). A calibration was previously carried out with buffers 4 and 7, then the pH was measured by inserting the tip in the form of a glass cone inside the fish and obtaining the corresponding values.

2.16. Determination of total volatile basic nitrogen (TVB-N)

The total volatile basic nitrogen (TVB-N) values of salmon were determined in accordance with the "Chilean standard norm NCh 2668:2018 for hydrobiological products. Briefly, 10 g of the fish

 doi:10.20944/preprints202312.1410.v1

sample, 2 g of magnesium oxide, and 100 mL of water were added to the distillation flask, followed by the distillation of the mixture. The distillate was taken up in 25 mL of a 3% m/v aqueous solution of boric acid and 5-7 drops of Tashiro's indicator (mixed indicator composed of a solution of methylene blue (0.1%) and methyl red (0.03%) in ethanol or methanol). Then, the boric acid solution was titrated to the endpoint with 0.1 N sulfuric acid.The

TVB-N content (mg of N/100 g) of fish sample was determined as follows:

$$\text{TVB} - \text{N} = \frac{\text{mL } H_2SO_4 \text{ 0.1N x 1.4 x 100}}{\text{Sample weight (g)}}$$

2.17. Microbiological analysis

As fish spoilage was being monitored by colorimetric indicators, samples were subjected to microbiological analysis at regular intervals. For total microbial count determination, 25 g of the salmon sample was added to 225 mL of 0.1% m/v peptone water. The mixture was homogenized in a homogenizer for 1 minute and the 0.1 dilution was obtained. From this dilution, further decimal dilutions were prepared and plated on Petri dishes in the appropriate media. Enumeration of total viable aerobic bacteria counts was performed according to the pour plate method using plate count agar (PCA) purchased from Merck. The inoculated Petri dishes were incubated at 35±1 ºC for 48 h to determine the mesophilic counts. Colony-forming unit (CFU) counts were expressed as CFU/g. All microbiological experiments were performed in duplicate.

2.18. Statistical analysis

The analyses and experiments were done in triplicate and the data were evaluated by analysis of variance (ANOVA) (comparison of several samples) using the PROGRAM-STATGRAPHICS Centurion XIX.v.64 followed by Fisher's Least Significant Difference (LSD) procedure. A probability level of $p<0.05$ will be considered statistically significant.

3. Results

3.1. Characterization of gold nanoparticles (AuNPs)

Gold nanoparticles were characterized by UV-VIS, infrared spectroscopy (FTIR), thermogravimetric analysis (TGA), differential scanning calorimetry (DSC), X-ray diffraction (XRD), transmission electron microscopy (TEM), and colorimetric analysis.

3.2. UV-Visible spectroscopy

In Figure 1, a color change of the solution was observed, it went from yellow to a red dispersion with the addition of trisodium citrate (NaCit), indicating the formation of gold nanoparticles [23]. In addition, it was possible to observe through the UV-VIS spectrum an absorption band at a wavelength of 520 nm in the red color of the spectrum that gives its hue, this phenomenon is related to surface plasmon resonance (SPR) because AuNP conduction electrons interact with incident photons to produce a resonance effect, manifested as SPR. This interaction depends on the size, shape, and composition of the metallic nanoparticles, as well as the type and content of the dispersion medium [24]. Similar results were obtained by [25].

Preprints (www.preprints.org) | NOT PEER-REVIEWED | Posted: 19 December 2023 doi:10.20944/preprints202312.1410.v1

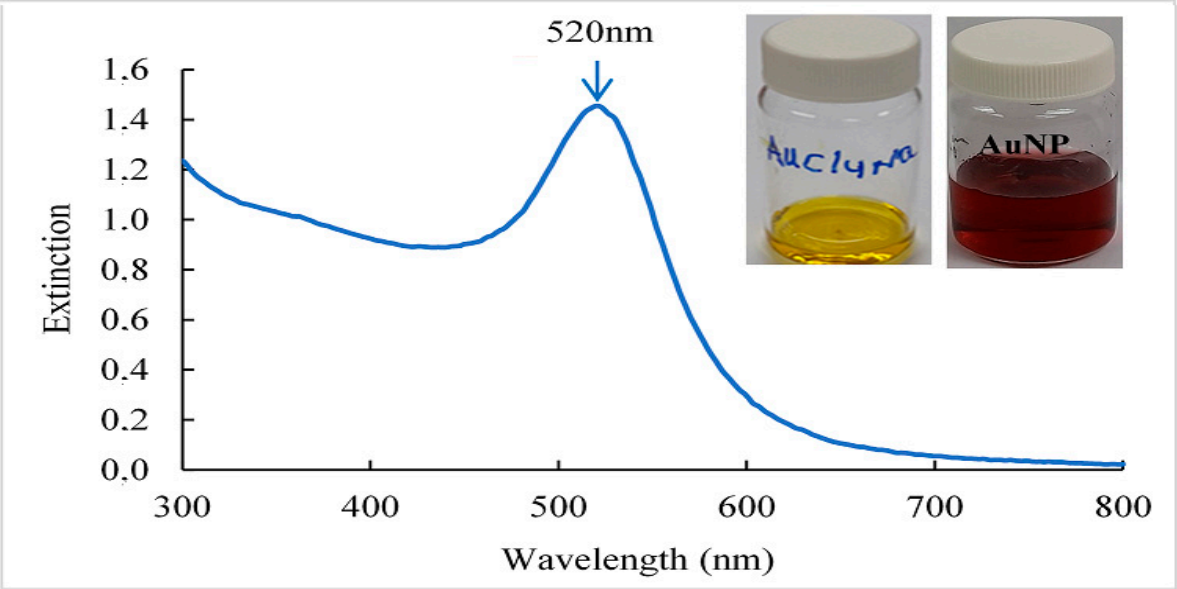

Figure 1. UV-Visible spectrum and photographs of gold nanoparticles (AuNP) obtained. Sodium tetrachloroaurate (NaAuCl4.2H2O) is used as a precursor of AuNP and NaCit ($C_6H_5Na_3O_7 \cdot 2H_2O$), as a reducer and stabilizer.

Figure 2 shows the result of the detection capacity of the AuNPs by UV-VIS spectrum, being able to observe two absorption peaks: the first peak is between 520 nm and 531nm, which may be associated with the aggregation of the AuNPs caused by their contact with the ETD solution. And the second absorption peak is located at a wavelength between 660 nm and 702 nm, which is associated with a change in the morphology of the AuNPs, because its union with the ETD produces a strong interaction between particles, varying their shape and size, as well as their color [26]. Similar results were reported by Sun et al. [27]. It should be noted that the bathochromic shift of AuNP results in a large displacement towards the red region of the Localized Surface Plasmon Resonance (LSPR) peak [28]. Furthermore, Mahatnirunkul et al. [29,30] affirmed that when the analyte of interest binds to the surface of AuNPs, the Localized Surface Plasmon Resonance (LSPR) spectrum will shift to a longer wavelength. Additionally, the aggregation of gold nanoparticles, after their contact with ethylenediamine occurred by the interaction of attractive van der Waals (VA) and repulsive Coulomb (VR) forces. Certainly, the gold nanoparticles in suspension remain stable when VR > VA. On the other hand, when VR < VA, nanoparticles clump together [31]. It has been detected that a wide variety of factors intervene in this process such as particle size, surface tension and, the electrical double layer, which have a high participation in reducing the stability of the NPs and their possible aggregation. However, in our case, citrate ions adsorb on the surface of the prepared AuNPs, creating a negative surface charge that stabilizes the particles; because the energy barrier was powerful enough to prevent strong interaction between particles and with that, it prevented them from aggregating. However, the addition of ETD to NaCit-stabilized AuNPs disturbed the stability of the nanoparticles by displacing the surrounding citrate layer, leading to aggregation.

Furthermore, when a higher AuNP extinction is observed, this is an indication of a higher concentration of nanoparticles. It should be noted that as the nanoparticles clump together, they increase in size, gradually settling to the bottom, resulting in less extinction. Similar results were obtained in previous studies by Ranjan et al. [32].

Preprints (www.preprints.org) | NOT PEER-REVIEWED | Posted: 19 December 2023 doi:10.20944/preprints202312.1410.v1

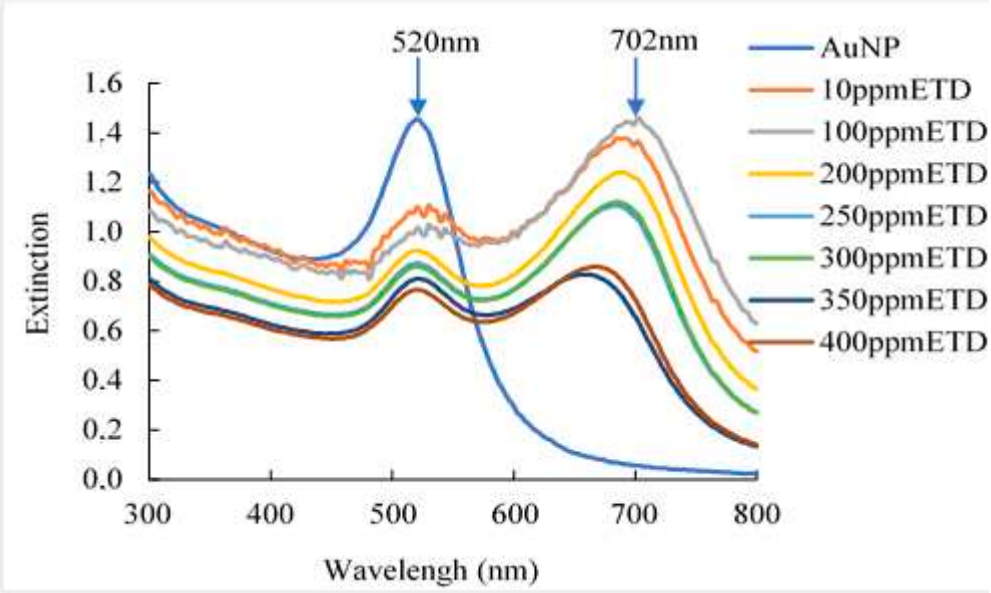

Figure 2. UV-VIS evaluation of the synthesized gold nanoparticles, based on different ETD concentrations (10-400ppm).

3.3. Transmission electron microscopy (TEM)

In order to study the size and morphology of synthesized AuNPs, TEM measurements were carried out. Figure 3a shows the TEM images of synthesized AuNPs, it can be observed that all the particles presented a homogeneous spherical shape and without agglomeration, as expected for this type of nanoparticles [33], in addition, it presents a wide size distribution from 10 to 16 and, 50 nm approximately.

On the other hand, in Figure 3b, it is shown that by adding ETD, the AuNPs aggregated and formed clusters due to a strong interparticle interaction. In addition, in the UV-VIS spectrum it was possible to corroborate a displacement of the wavelength towards the red region of the spectrum, indicating larger nanoparticles as demonstrated in the TEM analysis**Figure 2.** UV-VIS evaluation of the synthesized gold nanoparticles, based on different ETD concentrations (10-400ppm).

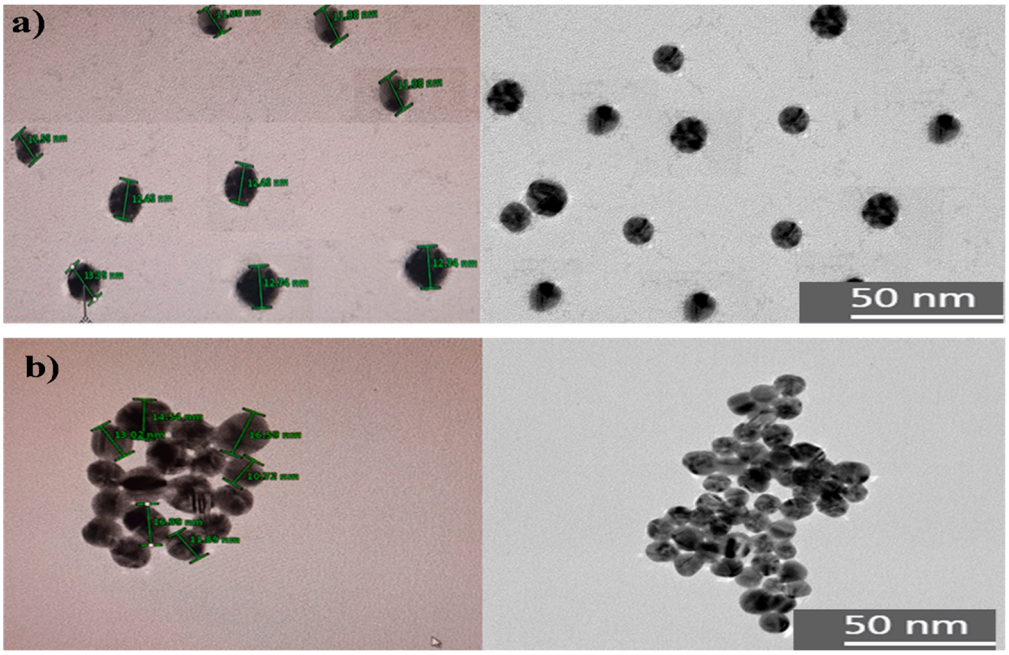

Figure 3. Images of a) AuNPs b) AuNP+ ETD (aggregated form).

Preprints (www.preprints.org) | NOT PEER-REVIEWED | Posted: 19 December 2023 doi:10.20944/preprints202312.1410.v1

3.3. Transmission electron microscopy (TEM)

In order to study the size and morphology of synthesized AuNPs, TEM measurements were carried out. Figure 3a shows the TEM images of synthesized AuNPs, it can be observed that all the particles presented a homogeneous spherical shape and without agglomeration, as expected for this type of nanoparticles [33], in addition, it presents a wide size distribution from 10 to 16 and, 50 nm approximately.

On the other hand, in Figure 3b, it is shown that by adding ETD, the AuNPs aggregated and formed clusters due to a strong interparticle interaction. In addition, in the UV-VIS spectrum it was possible to corroborate a displacement of the wavelength towards the red region of the spectrum, indicating larger nanoparticles as demonstrated in the TEM analysis

3.4. Infrared spectroscopy (FTIR) of trisodium citrate (NaCit) and AuNP

The FTIR analysis of Citrate-capped AuNPs is present in Figure 4 where it is possible to observe the presence of absorption bands at 1696, 1580, 1387, 1281, and 1079 cm^{-1}. The band at 1696 cm^{-1} is related to the COO− group originating due to the adsorption of citrate anions on gold nanoparticles through the central carboxylate group [31]. These two bands with their peaks at around 1387 and 1580 cm^{-1}, which respectively correspond to the symmetric ($\nu_s(COO^-)$) and antisymmetric ($\nu_{as}(COO^-)$) stretching bands of carboxyl groups of NaCit. For citrate-capped AuNP, the $\nu_{as}(COO^-)$ peak was found to be largely a high-frequency shift from the original peak position. In addition, absorption bands are observed between 1281-1079 cm^{-1} which corresponds to the stretching vibration of the C-O bond, as well as the C-C bond of NaCit [34,35]. The 3344cm^{-1} and 3446cm^{-1} absorption bands that appeared between 3600 and 3000 cm^{-1} are related to the stretching vibration of the O-H bond of NaCit. On the other hand, changes in the stretching vibration of the O-H group of the citrate were observed with the addition of AuNP. This was due to the interaction of the nanoparticles surrounded by the NaCit, giving rise to the formation of a new absorption band at wavenumber 3344cm^{-1}. This indicated the disappearance of the citrate band (3446cm^{-1}) evidencing the presence of gold nanoparticles [36].

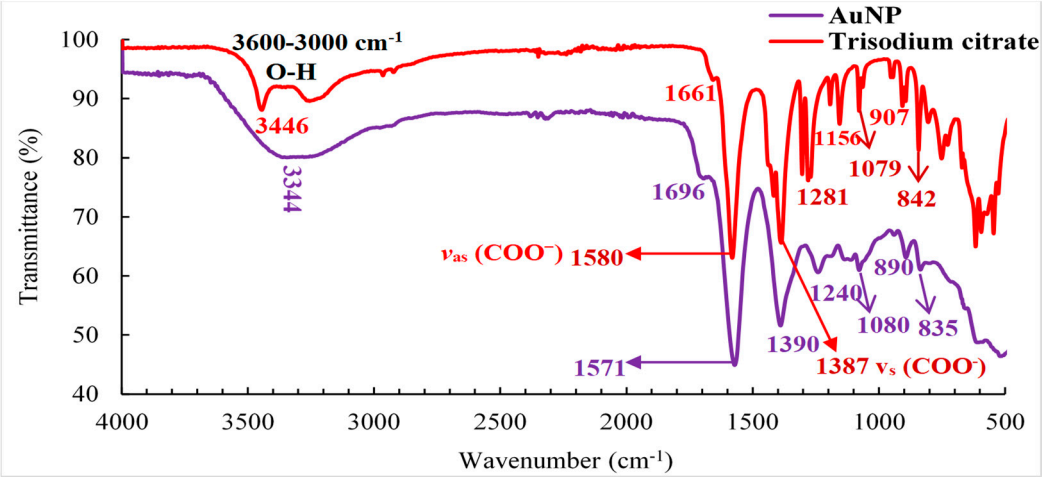

Figure 4. Infrared spectroscopy (FTIR) of AuNP functionalized with trisodium citrate.

3.5. Optical properties

In this experiment, AuNPs covered by a layer of negatively charged citrate ions were used that keep the nanoparticles well dispersed and stable in colloidal solution. The addition of ETD (Figure 5 and Table 1) caused an aggregation of AuNPs, mainly affecting the extinction spectrum with color changes of the AuNPs with a total color difference of ΔE =28.81. This aggregation could be due to an electrostatic interaction between the positively charged amine groups and the negatively charged trisodium citrate ion groups surrounding the AuNPs or could also be the result of some exchange between trisodium citrate ions and amines that probably can directly adhere to the AuNPs. These

 doi:10.20944/preprints202312.1410.v1

results indicated the ability of metallic nanoparticles to detect fish spoilage products by properly interacting with the test molecule, causing the formation of larger nanoparticles with subsequent color change in the dispersion.

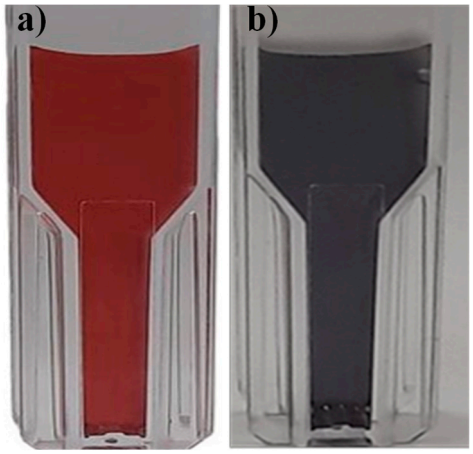

Figure 5. Colloidal solution of nanoparticles a) AuNP (red) b) AuNP+ETD (black).

Table 1. Color measurement of gold nanoparticles.

Color parameters	AuNP	AuNP+ETD
L*	10.56±0.48	9.96±0.40
a*	24.47±0.29	3. 17±0.24
b*	13.32±0.45	-6. 06±0.48
ΔE	---------	28.81

L* = lightness (0 = black, 100 = white), + b* (yellow), -b* (blue), + a*(red), -a*(green).

3.6. Thermogravimetric analysis

Figure 6 shows the TGA/DTGA of citrate-capped AuNP where 5 mass losses were observed. The first mass loss corresponds to the release of water from the sample and begins at 166 to 250ºC, representing 7.83% of the initial mass. The second mass loss is between 256°C and 336.5°C, with a peak at 288.5°C corresponding to a loss of 5.5%. The third endothermic peak is observed in the range of 375.3 °C to 482.6°C, with a peak at 437.3°C corresponding to a mass loss of 5.1%. The second and third peaks after the dehydration peak probably correspond to the degradation of the sample and/or organic matter covering the trisodium citrate. The fourth and fifth mass loss is observed in the temperature range 547ºC to 695.9ºC with peaks at 554.8ºC and 695.8ºC respectively. It is observed that in these last degradations, the losses are lower and are in the order of 0.18% and 0.27% respectively, which indicates that it would coincide with the final degradation of the trisodium citrate-capped gold nanoparticles. The total mass loss is equivalent to 18.9%. Similar results were obtained in previous studies [37].

Preprints (www.preprints.org) | NOT PEER-REVIEWED | Posted: 19 December 2023 doi:10.20944/preprints202312.1410.v1

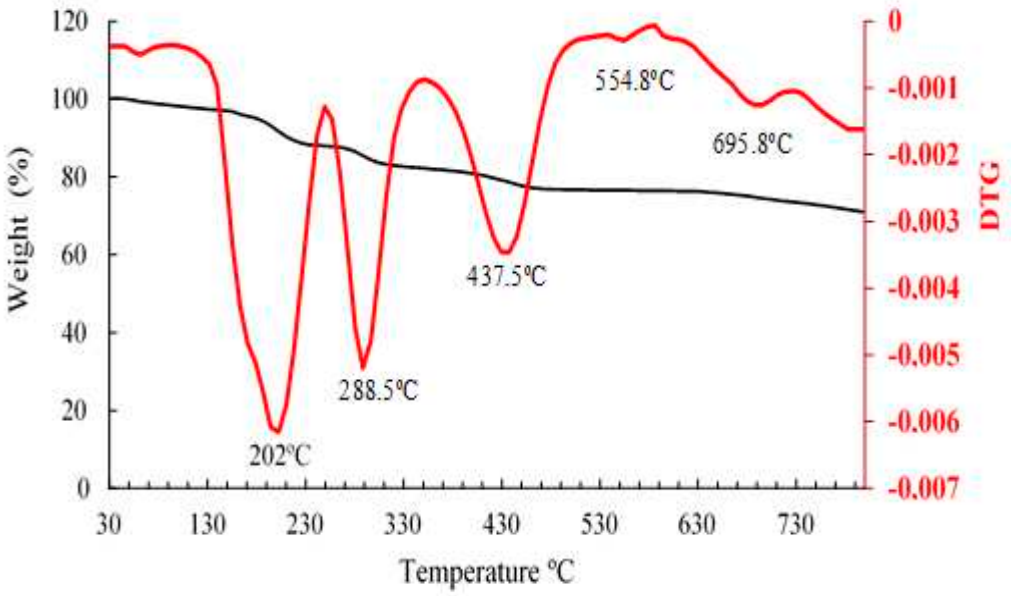

Figure 6. Thermogravimetric analysis TGA (black) and DTG (red) curves of citrate-capped AuNP.

3.7. Differential scanning calorimetry (DSC)

According to the DSC curve (Figure 7), it was observed that the citrate-capped AuNP in the first heating, shows endothermic peaks at 159.4, 176.4, 219.1, and 298.2 °C and an exothermic peak at 323.7 ºC where the latter corresponds to the crystallization of trisodium citrate. The first endothermic peak corresponds to the evaporation of adsorbed water . The second and third peaks could correspond to the beginning of the degradation of NaCit. The endothermic peak at 298.2ºC is related to the melting point of the NaCit that coats the surface of the gold nanoparticles. Similar results were obtained in previous studies by [38].

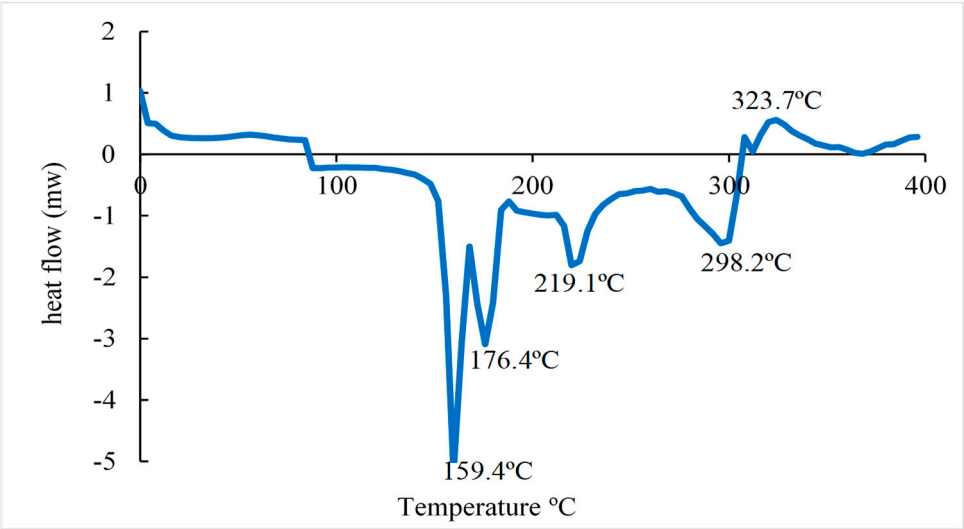

Figure 7. Differential scanning calorimetry analysis of gold nanoparticles (AuNP) capped by trisodium citrate.

3.8. X-ray diffraction analysis of AuNPs

The XRD patterns of the AuNPs (Figure 8) showed diffraction peaks at 2θ equal to 38.1º; 45.3º; 64.5º and 77.4º. These values match the corresponding (111), (200), (220), and (311) lattice planes of

Preprints (www.preprints.org) | NOT PEER-REVIEWED | Posted: 19 December 2023 doi:10.20944/preprints202312.1410.v1

AuNP and were in accordance with the Joint Committee on Powder Diffraction Standards (JCPDS) database no.04-0784 confirming the formation of AuNP. According to the results obtained, it is clear that the AuNPs formed are crystalline in nature [39]. These diffraction peaks may be the result of the capping agents that are responsible for the stabilization of the nanoparticles. Instead, a sharp peak is detected at 2θ=31.69º in the AuNPs, this could be due to the presence of citrate-capped AuNP. Likewise, the appearance of several other small less pronounced peaks was observed in the diffractograms of the AuNPs. This could be due to the presence of impurities in the analyzed samples.

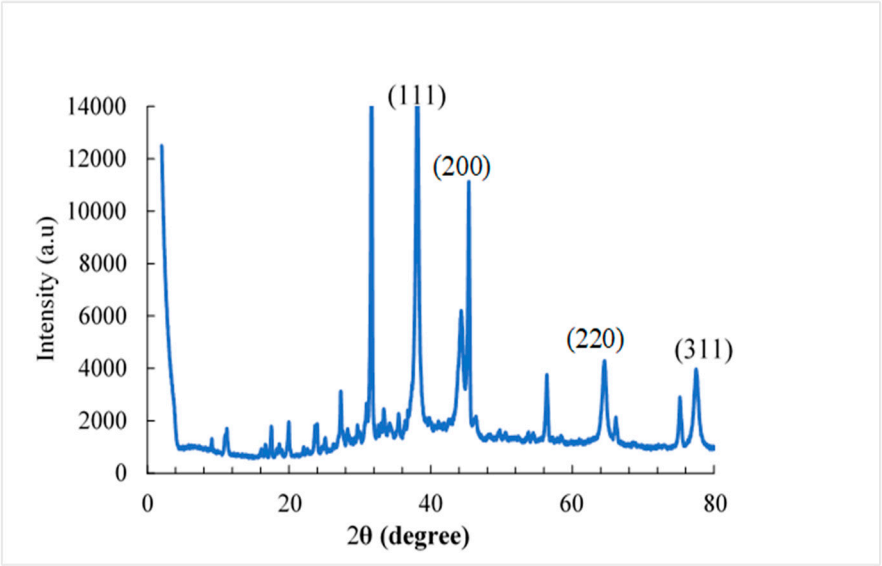

Figure 8. X-ray diffraction of synthesized AuNP capped by NaCit.

3.9. Development and Characterization of alginate bead-shaped indicator film

In Figure 9 you can see the result of the development of the indicator film (alginate bead shape) using the casting technique. Being able to observe the complete formation of the film based on gold nanoparticles and its *in vitro* evaluation with ethylenediamine, observing color changes after its reaction with the test molecule.

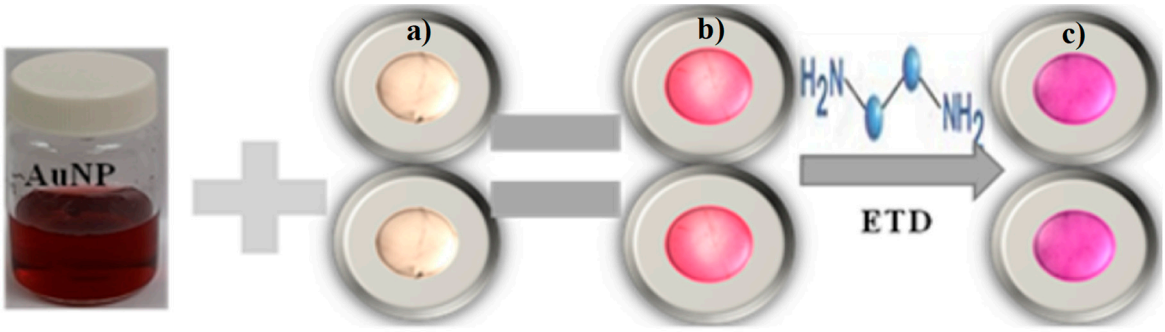

Figure 9. a) Sodium Alginate (Alg.) b) Indicator (Alg/AuNP). c) Indicator+ ETD. AuNP: gold nanoparticles. ETD: Ethylenediamine.

3.10. Infrared spectroscopy (FTIR)

In the FTIR spectra of the alginate beads (Figure 10), a large absorption band was observed in the range of 3600 to 3000 cm^{-1} related to the stretching vibration of the OH group and the C-H vibration bands at 2935 cm^{-1}. The bands observed at 1594 cm^{-1} and 1415 cm^{-1} were attributed to the asymmetric and symmetric stretching vibrations of the COO^- groups of Alg, respectively, and are

Preprints (www.preprints.org) | NOT PEER-REVIEWED | Posted: 19 December 2023 doi:10.20944/preprints202312.1410.v1

specific for ionic bonding. The shoulder located at 1080 cm^{-1} related to C–C and C–O stretching can also be attributed to crossover. The absorption band detected at (1027 ± 4 cm^{-1}) shows a higher intensity in relation to the 1080 cm^{-1} band, suggesting a stronger O-H binding vibration or a stronger binding of Ca^{2+} to guluronic acids from the sodium alginate. In contrast, the stretching vibration bands observed at approximately 939 cm^{-1} and 889 cm^{-1} are specific for guluronic and mannuronic acids. Also, small displacements of the carboxyl groups were observed, which may be indicative of an ionic union between Ca^{2+} and sodium alginate chains [41]. In addition, in the evaluation of the colorimetric indicator with ETD a crossover is observed in the stretching of the O-H group in the range of 3600-3000 cm^{-1}. This is due to the reaction of the ETD with the carboxyl group of the NaCit on the surface of the gold nanoparticles, causing the nanoparticles to clump together. That led to the appearance of new bands in the indicated range.

On the other hand, it is known that sodium alginate is a polymer with a strong hydrophilic character [42], so its contact with the ethylenediamine solution and the modifications provided by the gold nanoparticles in its structure could produce a crossover.

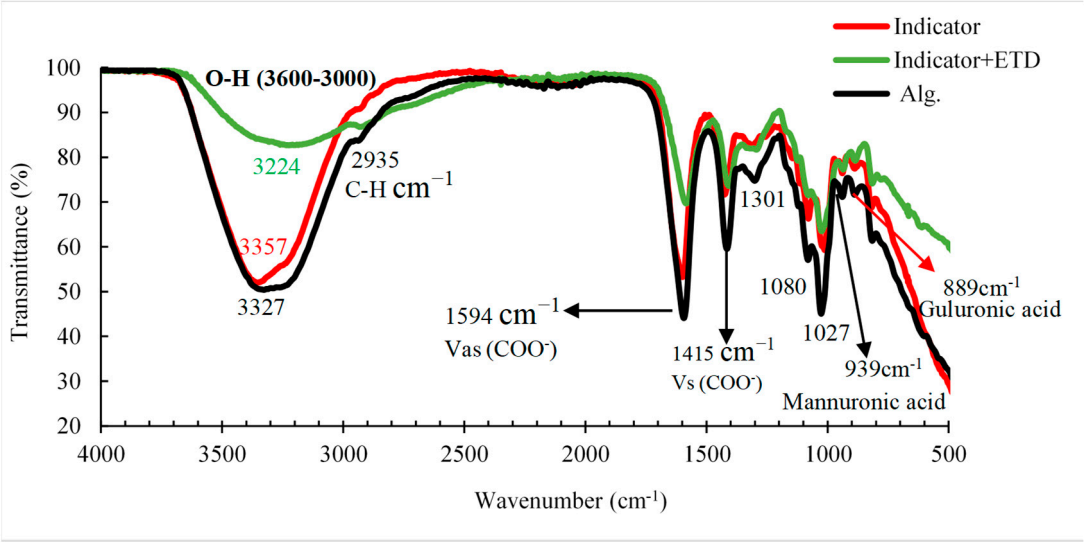

Figure 10. Infrared spectroscopy (FTIR) of Indicator (Alg./AuNP) ; Indicator+ ETD and Alg.

3.11. Analysis of thermal stability

In Figure 11 and Table 2, four main stages or successive losses can be seen in the thermograms. In the first stage, the weight loss occurred at the beginning of the heat treatment, in the range of 47.8°C to 168.8°C, mainly attributed to the loss of free water absorbed by sodium alginate and the indicator [43]. The second stage of thermal degradation was sensed at the onset of the temperature ranging from about 171.8 to 291.4ºC associated with the thermal degradation of the polymer as well as the polymer capping around the nanoparticles. While the third and fourth weight loss could be related to the conversion of the remaining polymer into carbon residues [44] in the case of sodium alginate. However, in the colorimetric indicator, the third and fourth losses could correspond to the degradation of the citrate and the residual compounds present in the sample. It was observed that the colorimetric indicator with a mass loss of 45.6% presented certain thermal stability in relation to alginate and its evaluation with ETD. This is because the incorporation of AuNP destabilized the beads due to the increased negative charge density in the hydrogel matrix [45]. Moreover, it was observed that there was a greater mass loss (54.8%) in the control (Alg) with respect to the colorimetric indicator and its reaction with ETD, respectively, because sodium alginate is a hydrophilic polyanion and sensitive to pH [46].

On the other hand, a similar mass loss of 45.6% and 44.5% was observed in the colorimetric indicators without and with ETD. This mass loss could be due to the interaction of the amino group (NH_2) of the ETD with the carboxyl group (COO^-) of the oxygen-starved NaCit surrounding the

Preprints (www.preprints.org) | NOT PEER-REVIEWED | Posted: 19 December 2023 doi:10.20944/preprints202312.1410.v1

AuNPs leading to cluster formation that could, to some extent, decrease the resistance to the temperature of the colorimetric indicator until it degrades above 700ºC. No significant difference was observed between the lost masses (p≥0.05).

Table 2. TGA analysis results of Alg, colorimetric indicator, and indicator with ETD.

Samples	Temperature (ºC)	T-onset (ºC)	T50 (ºC)	T endset (ºC)	Mass lost (%)
Sodium Alginate (Alg.)	30-800	49.4	110.5	168.8	23.4±1.3
		172.8	190	243.7	15.8±1.6
		246.5	290.6	316.7	11.1±0.4
		388.3	417.9	460.3	4.4±0.5
Indicator (Alg+AuNP)	30-800	47.8	111.3	153.9	22.2±4
		172.1	201	237.4	9.4±0.7
		239.1	276.2	314.4	12±1.6
		347.8	371.8	397. 2	1.7±0.3
Indicator with ETD	30-800	49.5	95.8	141.2	19.9±4
		207.1	251.7	291.4	19±4.6
		375.2	424.3	445.5	3.6±0.6
		637.6	673.5	729.8	1.9±0.3

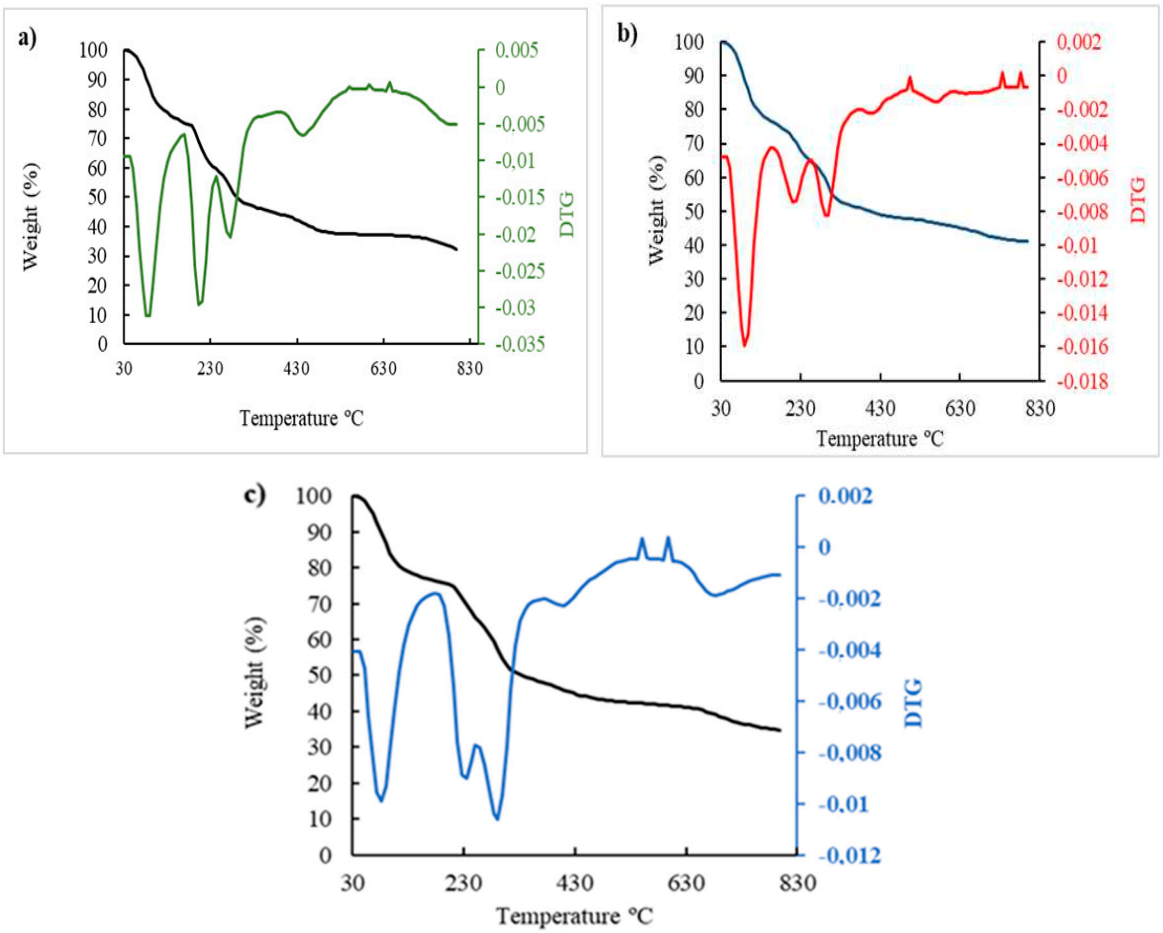

Figure 11. Thermogravimetric analysis of **a)** Sodium Alginate (Alg.) TGA (**black**) DTG (**green**). **b)** Indicator (Alg./AuNP) TGA **(black)** DTG **(red)** and **c)** Indicator + ETD-TGA **(black)**, DTG **(blue).**

3.12. Differential scanning calorimetry (DSC)

The DSC analysis curves reflect the thermal properties of the control alginate (Alg.), of the colorimetric indicator, and its evaluation with ETD. The endothermic melting peak of water

Preprints (www.preprints.org) | NOT PEER-REVIEWED | Posted: 19 December 2023 doi:10.20944/preprints202312.1410.v1

crystallization appeared at 100.7, 103.6, and 106.9°C in sodium alginate, colorimetric indicator and indicator with ETD respectively (Figure 12). The results obtained from the current experiment do not present significant differences ($p \geq 0.05$) in any of the analyzed indicators nor in the control, with the exception of a greater broadening of the water absorption peak in the evaluated indicator with ETD that could be due to the hydrophilic behavior of sodium alginate [47] and/or the formation of new chemical bonds and interaction between the components of the *in vitro* assessed colorimetric indicator. Additionally, the enthalpy of fusion (ΔH) of the control (Alg.) (-536.7J/g) was higher than that of the colorimetric indicator (-1217.8 J/g) and indicator with ETD (-556.9 J/g). This could indicate that AuNP with the analyte causes a reduction in this parameter. Chen et al. showed analogous results in evaluating the thermal property (DSC) of alginate with the addition of thymol [48].

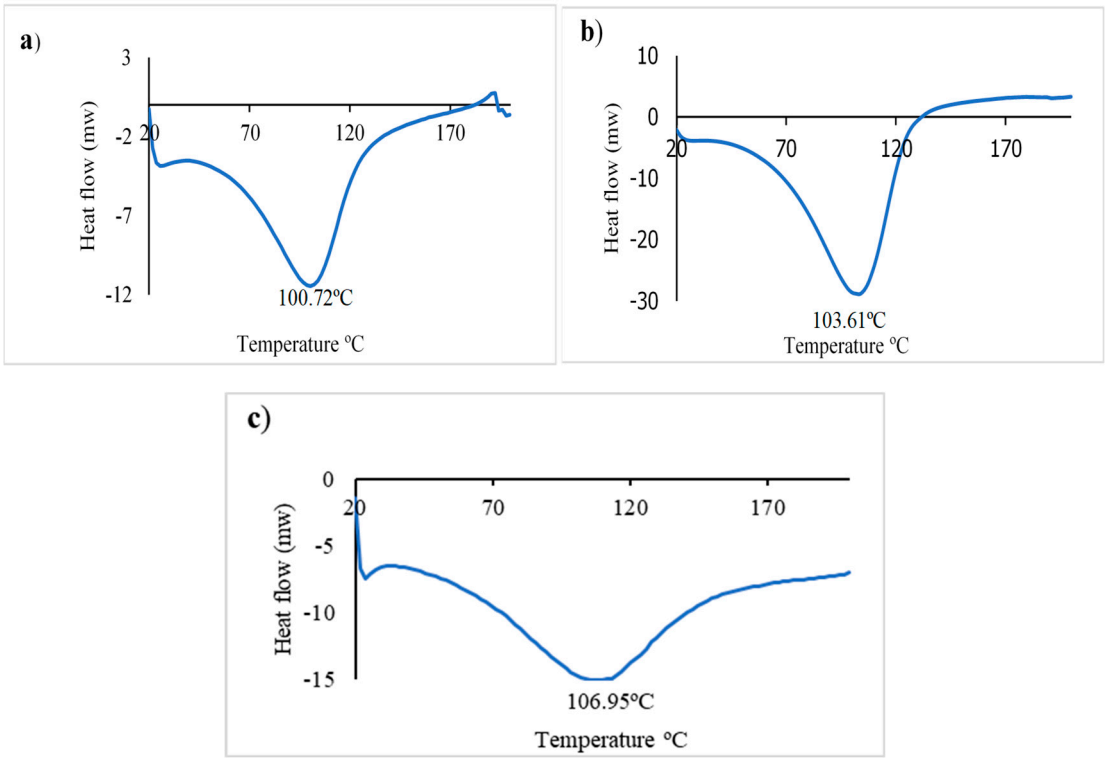

Figure 12. Differential scanning calorimetry DSC **a**) Sodium Alginate (Alg.) **b**) Indicator (Alg./AuNP) **c**) Indicator + ETD.

3.13. XRD analysis

XRD diffractograms of Alg., colorimetric indicator, and its assessment with ETD are presented in Figure 13. In the diffraction patterns of Alg., it was observed that it presented two characteristic diffraction peaks at 2θ =12.8° and 20.3 indicating a certain level of crystallinity. Similar results were reported by [49].

On the other hand, the colorimetric indicator did not show the appearance of a peak. This may be indicative of the amorphous nature of the colorimetric indicator, since AuNPs can modify the semi-crystalline structure of the alginate, turning it into a fully amorphous structure. Similar results were informed by [50].

In other ways, the results obtained from the colorimetric indicator with ETD presented 2 peaks at 2θ=16.4° and 22.7° associated with the semicrystalline structure of the indicator evaluated with Ethylenediamine.

Preprints (www.preprints.org) | NOT PEER-REVIEWED | Posted: 19 December 2023 doi:10.20944/preprints202312.1410.v1

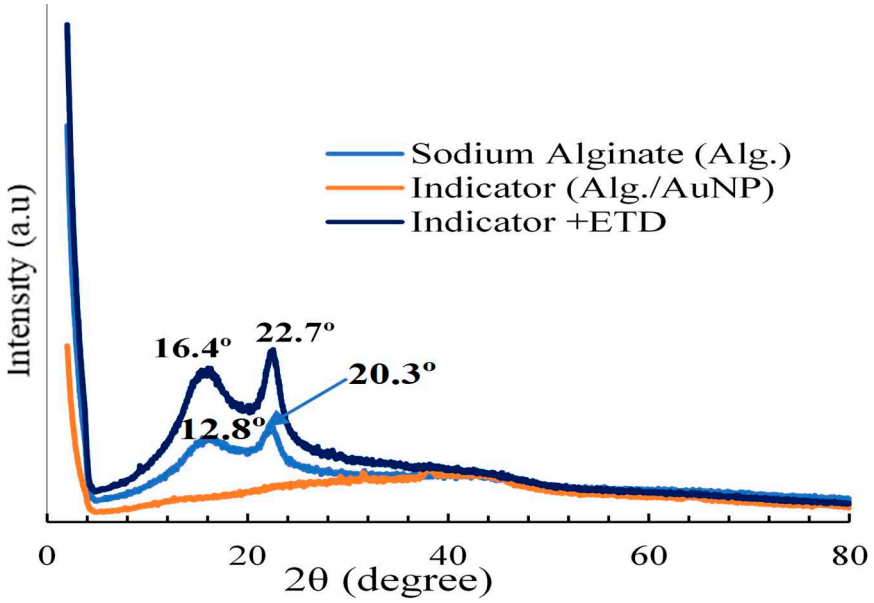

Figure 13. X-ray diffraction of Sodium Alginate; Indicator and Indicator+ ETD.

3.14. Determination of total volatile basic Nitrogen (TVB-N)

Volatile compounds such as trimethylamine, ammonia, and dimethylamine produced by the destructive activities of microorganisms are considered one of the most important parameters to determine the quality and freshness of fish and are known as total volatile basic nitrogen (TVB-N) [51]. According to the results (Figure 14), the initial values of TVB-N were 13.3 and 13.8 in the colorimetric indicator and control respectively and they coincided correctly with the low initial microbial counts. These values are similar to results obtained in previous research [52]. However, the TVB-N content increased progressively from 13.3 to 45.9 mg/100g and from 13.8 to 44.8 mg N/100g in colorimetric indicator and control respectively after 9 days of storage at 5°C. This increase may be due to: 1) the activity of spoilage bacteria that grow in the fish 2) the enzymatic reaction that can occur in stored muscle food [53] 3) and, to autolysis. A comparison of TVB-N values with colorimetric analysis shows that the color change of the colorimetric indicator is proportional to TVB-N content and pH change. The increase in the amount of TVB-N caused an increase in pH and a color change in the colorimetric indicator.

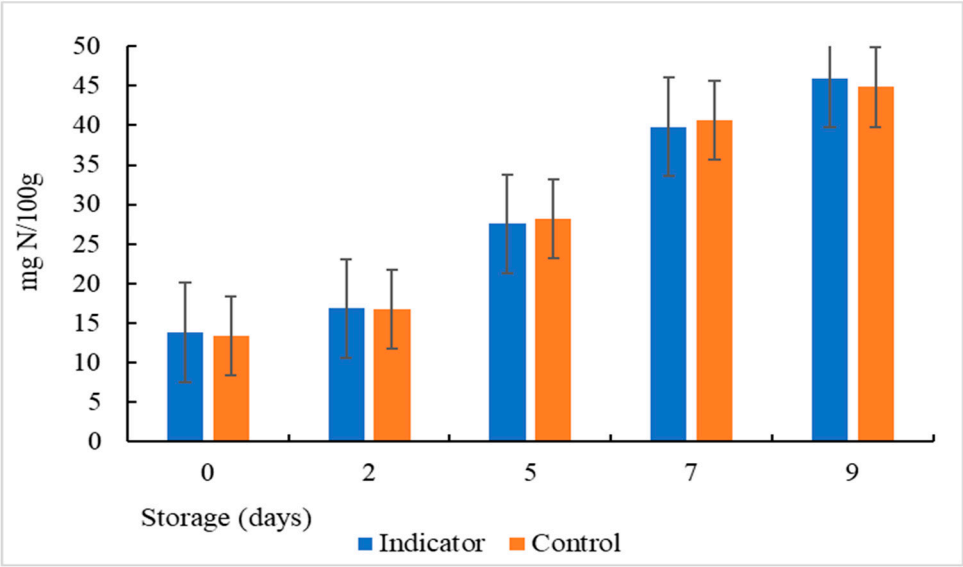

Figure 14. Determination of total volatile basic nitrogen (TVB-N) in fish stored at 5ºC.

 doi:10.20944/preprints202312.1410.v1

3.15. Mesophilic aerobic count

Changes in aerobic bacteria counting in salmon samples stored at 5°C are shown in Figure 15. Initial Aerobic Mesophyll Count (AMC) values for marine fish prior to cold storage typically range from 2 to 4 $\log_{10}$ CFU/g, and a value of 6 $\log_{10}$ CFU/g is considered the upper limit of acceptability [54]. Therefore, the values obtained 2.82 and 2.80 $\log_{10}$ CFU/g for the control and the sample with the colorimetric indicator in this study are within this range. This indicates the freshness of the salmon with a low microorganism count. However, the bacteria grow gradually until reaching a value of 6.8 $\log_{10}$ CFU/g on the seventh day and can reach values greater than 9 $\log_{10}$ CFU/g on the ninth day of storage (data not shown) at a temperature of 5ºC. This growth of microorganisms leads to greater production of biogenic amines, changes in the pH value, and deterioration of the fish. However, there was no significant difference ($p \geq 0.05$) in the growth of the bacteria between the control (fish sample only) and the sample with an colorimetric indicator inserted so that they grow at the same rate. Similar results were obtained in evaluating the spoilage potential of *P. fluorescens* in salmon at different temperatures [55]. According to previous studies, the bacteria that grow more at refrigeration temperatures are the so-called psychotropics. Also, Pseudomonas spp. was suggested as the main specific spoilage organism [56] and it is useful to predict shelf life with a cut-off level of 6.5 $\log_{10}$ CFU/g. Cheng and Sun reported that the main group of bacteria causing spoilage of refrigerated or modified atmosphere vacuum-packed fish products are lactic acid bacteria such as *lactobacillus, Streptococcus, Leuconostoc, and Pediococcus spp.* These bacteria are capable of spoiling foods by fermenting sugars and commonly cause undesirable defects such as off-flavors, discoloration, gas production, slime production, and lowering of pH [57]. In addition, they are capable of inhibiting the growth of other bacteria due to the formation of lactic acid and bacteriocins, and this facilitates their selective growth during fish spoilage [58].

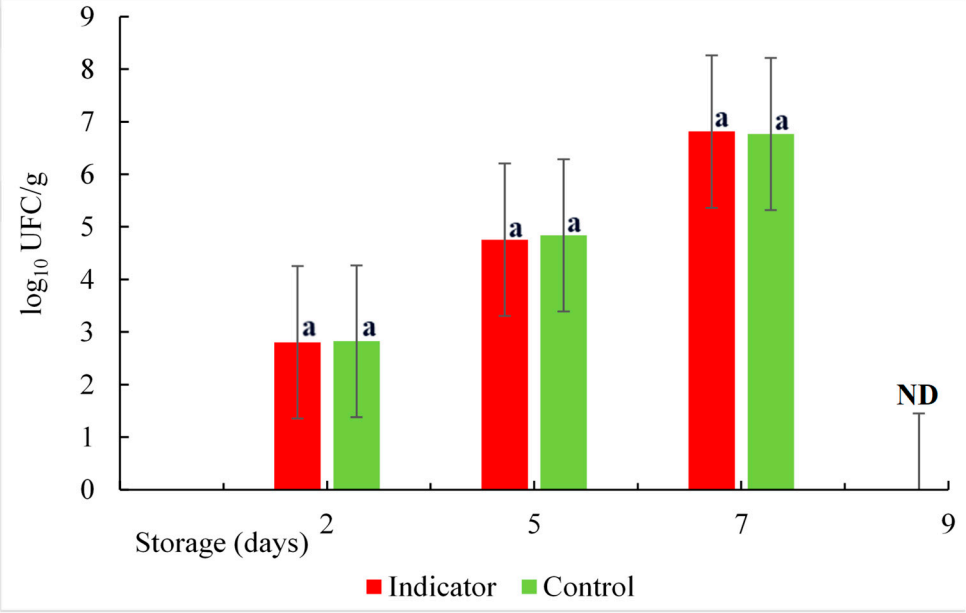

Same lowercase letters in each day indicate no statistically significant differences.

Figure 15. Count of Mesophilic Aerobes as a function of time.**ND** : not determined.

3.16. Determination of pH

The changes in the pH values during storage were presented in Figure 16 where a decrease in the pH value was observed on day 2 of storage. This may be related to the production of some acidic substances because both the skin and the digestive system of fish can host a variety of bacteria, among which are lactic acid bacteria, which are facultatively anaerobic and grow very well under microaerophilic conditions [59]. These bacteria produce lactic acid as the main metabolic end product

Preprints (www.preprints.org) | NOT PEER-REVIEWED | Posted: 19 December 2023 doi:10.20944/preprints202312.1410.v1

of carbohydrate consumption. When the lactic acid population increases during storage, there is an increase in lactic acid capable of neutralizing alkaline amine products, thus reducing the pH [58] Undoubtedly, lactic acid bacteria predominated in the total natural microflora of the vacuum-packed fish fillets. On the other hand, another factor of a drop in pH could be the by-products of lipid oxidation caused by the reaction of amine compounds with aldehydes. Similar results were obtained in previous investigations [54]. However, on days 7 and 9 of storage, variations in pH values from 7.54 and 7.92 to 9.45 and 9.60 were observed for the colorimetric indicator and the control, respectively. This is due to an increase in the growth of microorganisms in the muscle food, producing an increase in the TVB-N values and pH changes.

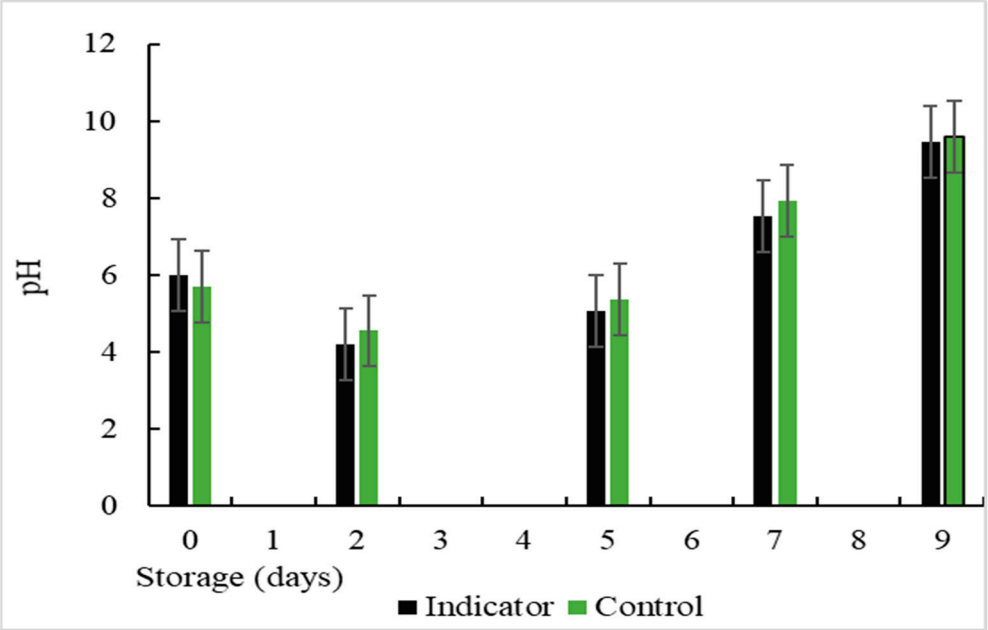

Figure 16. Changes in the pH value during storage at a temperature of 5ºC.

3.17. Indicator color measurement

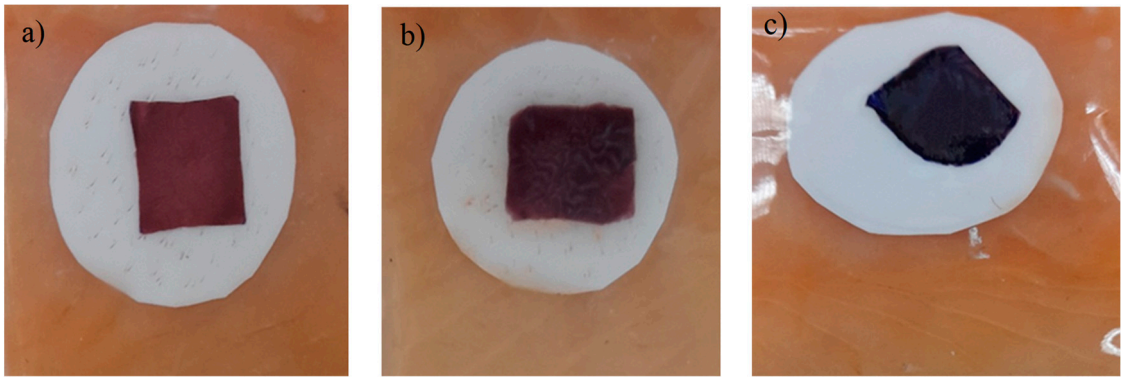

Figure 17. Color changes of the colorimetric indicator in fish stored at 5ºC. a) day 0. b) day 7.c) day 9.

The color parameters for the colorimetric indicators based on metallic nanoparticles were determined. According to Table 3, a* values decreased from 33 (redder) to 13 (greener) after 9 days of storage at refrigeration temperature. This means that the red color had a lower intensity at the end of the storage period. The values recorded for b* decreased from 13 to -24.11 indicating that the blue color appeared more pronounced at the end of the storage period. However, it is observed that the blue color began to appear from days 5 to 9 of storage, therefore, it is obvious that the blue color predominates in the evaluation of the colorimetric indicator. Researchers reported that a ΔE^* value

 doi:10.20944/preprints202312.1410.v1

greater than 4 can be easily detected with the naked eye, while values greater than 12 imply a complete color difference that is detectable even by untrained panelists [60]. Therefore, ΔE^* of the colorimetric indicators obtained in the current experiment can be detected by the human eye during fish storage. Generally, indicators used as a colorimetric sensor exhibit a wide range of color variations depending on the pH which can be affected by the TVB-N content during the storage period. This has the obvious advantage that color changes can be inspected with the naked eye to detect the rate of spoilage packaged fish. On the other hand, a progressive increase of the ΔE parameter was observed until the end of the storage time, this can be attributed to the loss of water that occurs as time passes, which would give rise to greater water deposits on the surface of the fish, which inevitably leads to a variation in the value of this parameter.

When comparing the total color differences **(ΔE)** (Table 3) from the second to the last day of storage, it was observed that there are significant differences in the color of the colorimetric indicators analyzed with $p \leq 0.05$.

Table 3. Indicator colorimetric analysis.

Storage times (days)	L*	a*	b*	ΔE
0	17.86±3.57	33.47±4.09	13.01±3.94	-
2	9.60±0.32	12.42±2.09	0.80±0.75	25.7
5	21.23±0.48	15.85±0.26	-3.27±0.13	24.6
7	16.92±0.53	11.31± 0.18	-2.88±0.45	27.7
9	8.86±0.61	13.73±1.04	-24.11±1.01	43.1

L* = lightness (0 = black, 100 = white), + b* (yellow), -b* (blue), + a*(red), -a*(green).
ΔE= total color difference.

4. Conclusions

In this study, a new colorimetric indicator was developed using bead-shaped alginate containing gold nanoparticles to monitor fish spoilage. The colorimetric indicator was found to be sensitive to changes in pH and volatile amines produced during the storage of the fish. Results from visual inspection and CIELab colorimetric analysis of the colorimetric indicator were found to agree well with TVB-N values and microbial growth patterns, which can be used as indicators of spoilage in fish and other protein-rich food products.

The advantages of this colorimetric indicator are its easy manufacture and application, as well as the low cost of materials, such as sodium alginate and stomach bags, are among the advantages of the colorimetric indicator developed in this study that makes them especially useful for its application in smart packaging.

The disadvantage of this system is the instability of the alginate in the presence of water because it is a hydrophilic polymer, it tends to absorb water when stored in a humid environment for a long period. However, it may present greater stability depending on the storage conditions of the fish and its derived products. In conclusion, the gold nanoparticles-based colorimetric indicator system is suitable for monitoring the quality of refrigerated foods such as fish and meat.

Author Contributions: Conceptualization, Lissage Pierre.; methodology, Julio Bruna and Lissage Pierre; validation, Julio Bruna.; Patricio Leyton.; formal analysis, Lissage Pierre.; investigation, Lissage Pierre.; resources, Julio Bruna and ANID.; Data curation, Lissage Pierre.; writing-original draft preparation, Lissage Pierre.; writing-review and editing, Lissage Pierre ; Julio Bruna; Patricio Leyton; Alejandra Torres and Francisco Rodriguez.; visualization, Julio Bruna and Patricio Leyton.; supervision, Julio Bruna.; Project administration,

Lissage Pierre.; Funding acquisition, Julio Bruna and Lissage Pierre. All authors have read and agreed to the published version of the manuscript.

Funding: Funding: This research was funded by National Research and Development Agency (ANID) through the National Doctoral Scholarship and the Center of Excellence with Basal Financing (CEDENNA), grant AFB220001.

Institutional Review Board Statement: Not applicable.

Data Availability Statement: Not applicable.

Acknowledgments : The authors are also grateful to the University of Santiago de Chile for the Foreigner grant and Research Support grant (Ph.D. (c) Lissage Pierre).

References

1. J. K. G. Pataca, P. Porto-Figueira, J. A. M. Pereira, H. Caldeira, and J. S. Câmara, "Profiling the occurrence of biogenic amines in different types of tuna samples using an improved analytical approach," *LWT*, vol. 139, Mar. 2021, doi: 10.1016/j.lwt.2020.110804.
2. P. Visciano, M. Schirone, and A. Paparella, "An overview of histamine and other biogenic amines in fish and fish products," *Foods*, vol. 9, no. 12. MDPI AG, Dec. 01, 2020. doi: 10.3390/foods9121795.
3. X. Zhai *et al.*, "A colorimetric hydrogen sulfide sensor based on gellan gum-silver nanoparticles bionanocomposite for monitoring of meat spoilage in intelligent packaging," *Food Chem*, vol. 290, pp. 135–143, Aug. 2019, doi: 10.1016/j.foodchem.2019.03.138.
4. D. Doeun, M. Davaatseren, and M. S. Chung, "Biogenic amines in foods," *Food Science and Biotechnology*, vol. 26, no. 6. The Korean Society of Food Science and Technology, pp. 1463–1474, Dec. 01, 2017. doi: 10.1007/s10068-017-0239-3.
5. F. Barbieri, C. Montanari, F. Gardini, and G. Tabanelli, "Biogenic amine production by lactic acid bacteria: A review," *Foods*, vol. 8, no. 1. MDPI Multidisciplinary Digital Publishing Institute, 2019. doi: 10.3390/foods8010017.
6. Y. Xu, J. Zang, J. M. Regenstein, and W. Xia, "Technological roles of microorganisms in fish fermentation: a review," *Critical Reviews in Food Science and Nutrition*, vol. 61, no. 6. Bellwether Publishing, Ltd., pp. 1000–1012, 2021. doi: 10.1080/10408398.2020.1750342.
7. O. Comas-Basté, M. L. Latorre-Moratalla, S. Sánchez-Pérez, M. T. Veciana-Nogués, and M. del C. Vidal-Carou, "Histamine and other biogenic amines in food. From scombroid poisoning to histamine intolerance," *Biog Amines*, vol. 1, 2019.
8. M. Fusek, J. Michálek, L. Buňková, and F. Buňka, "Modelling biogenic amines in fish meat in Central Europe using censored distributions," *Chemosphere*, vol. 251, Jul. 2020, doi: 10.1016/j.chemosphere.2020.126390.
9. M. Senapati and P. P. Sahu, "Onsite fish quality monitoring using ultra-sensitive patch electrode capacitive sensor at room temperature," *Biosens Bioelectron*, vol. 168, Nov. 2020, doi: 10.1016/j.bios.2020.112570.
10. M. Ghaani, C. A. Cozzolino, G. Castelli, and S. Farris, "An overview of the intelligent packaging technologies in the food sector."
11. P. Müller and M. Schmid, "Intelligent packaging in the food sector: A brief overview," *Foods*, vol. 8, no. 1. MDPI Multidisciplinary Digital Publishing Institute, 2019. doi: 10.3390/foods8010016.
12. X. Luo, A. Zaitoon, and L. T. Lim, "A review on colorimetric indicators for monitoring product freshness in intelligent food packaging: Indicator dyes, preparation methods, and applications," *Compr Rev Food Sci Food Saf*, vol. 21, no. 3, pp. 2489–2519, May 2022, doi: 10.1111/1541-4337.12942.
13. M. Majdinasab, S. M. H. Hosseini, M. Sepidname, M. Negahdarifar, and P. Li, "Development of a novel colorimetric sensor based on alginate beads for monitoring rainbow trout spoilage," *J Food Sci Technol*, vol. 55, no. 5, pp. 1695–1704, May 2018, doi: 10.1007/s13197-018-3082-5.
14. T. Lin, Y. Wu, Z. Li, Z. Song, L. Guo, and F. Fu, "Visual monitoring of food spoilage based on hydrolysis-induced silver metallization of au nanorods," *Anal Chem*, vol. 88, no. 22, pp. 11022–11027, Nov. 2016, doi: 10.1021/acs.analchem.6b02870.
15. E. Taherkhani, M. Moradi, H. Tajik, R. Molaei, and P. Ezati, "Preparation of on-package halochromic freshness/spoilage nanocellulose label for the visual shelf life estimation of meat," *Int J Biol Macromol*, vol. 164, pp. 2632–2640, Dec. 2020, doi: 10.1016/j.ijbiomac.2020.08.177.
16. L. Wang, Z. Wu, and C. Cao, "Technologies and fabrication of intelligent packaging for perishable products," *Applied Sciences (Switzerland)*, vol. 9, no. 22. MDPI AG, Nov. 01, 2019. doi: 10.3390/app9224858.
17. L. Ding *et al.*, "A naked-eye detection polyvinyl alcohol/cellulose-based pH sensor for intelligent packaging," *Carbohydr Polym*, vol. 233, Apr. 2020, doi: 10.1016/j.carbpol.2020.115859.
18. M. K. Morsy *et al.*, "Development and validation of a colorimetric sensor array for fish spoilage monitoring," *Food Control*, vol. 60, pp. 346–352, Feb. 2016, doi: 10.1016/j.foodcont.2015.07.038.

19. K. M. A. El-Nour, E. T. A. Salam, H. M. Soliman, and A. S. Orabi, "Gold Nanoparticles as a Direct and Rapid Sensor for Sensitive Analytical Detection of Biogenic Amines," *Nanoscale Res Lett*, vol. 12, no. 1, Dec. 2017, doi: 10.1186/s11671-017-2014-z.
20. I. Dudnyk, E. R. Janeček, J. Vaucher-Joset, and F. Stellacci, "Edible sensors for meat and seafood freshness," *Sens Actuators B Chem*, vol. 259, pp. 1108–1112, Apr. 2018, doi: 10.1016/j.snb.2017.12.057.
21. X. Zhai *et al.*, "Novel colorimetric films based on starch/polyvinyl alcohol incorporated with roselle anthocyanins for fish freshness monitoring," *Food Hydrocoll*, vol. 69, pp. 308–317, 2017.
22. H. zhi Chen, M. Zhang, B. Bhandari, and C. hui Yang, "Novel pH-sensitive films containing curcumin and anthocyanins to monitor fish freshness," *Food Hydrocoll*, vol. 100, Mar. 2020, doi: 10.1016/j.foodhyd.2019.105438.
23. T. Patil, R. Gambhir, A. Vibhute, and A. P. Tiwari, "Gold nanoparticles: Synthesis methods, functionalization and biological applications," *J Clust Sci*, vol. 34, no. 2, pp. 705–725, 2023.
24. S. J. Nadaf *et al.*, "Green synthesis of gold and silver nanoparticles: Updates on research, patents, and future prospects," *OpenNano*, vol. 8. Elsevier Inc., Nov. 01, 2022. doi: 10.1016/j.onano.2022.100076.
25. R. Herizchi, E. Abbasi, M. Milani, and A. Akbarzadeh, "Current methods for synthesis of gold nanoparticles," *Artif Cells Nanomed Biotechnol*, vol. 44, no. 2, pp. 596–602, Jan. 2016, doi: 10.3109/21691401.2014.971807.
26. C. C. Chang, C. P. Chen, T. H. Wu, C. H. Yang, C. W. Lin, and C. Y. Chen, "Gold nanoparticle-based colorimetric strategies for chemical and biological sensing applications," *Nanomaterials*, vol. 9, no. 6. MDPI AG, Jun. 01, 2019. doi: 10.3390/nano9060861.
27. J. Sun, Y. Lu, L. He, J. Pang, F. Yang, and Y. Liu, "Colorimetric sensor array based on gold nanoparticles: Design principles and recent advances," *TrAC - Trends in Analytical Chemistry*, vol. 122. Elsevier B.V., Jan. 01, 2020. doi: 10.1016/j.trac.2019.115754.
28. A. N. D. Kolb and J. H. Johnston, "Colour tuneable anisotropic, water-dispersible gold nanoparticles stabilized by chitosan," *Gold Bull*, vol. 49, no. 1–2, pp. 1–7, Sep. 2016, doi: 10.1007/s13404-016-0176-6.
29. T. Mahatnirunkul, D. C. Tomlinson, M. J. McPherson, and P. A. Millner, "One-step gold nanoparticle size-shift assay using synthetic binding proteins and dynamic light scattering," *Sens Actuators B Chem*, vol. 361, Jun. 2022, doi: 10.1016/j.snb.2022.131709.
30. J. H. Lin and W. L. Tseng, "Ultrasensitive detection of target analyte-induced aggregation of gold nanoparticles using laser-induced nanoparticle Rayleigh scattering," *Talanta*, vol. 132, pp. 44–51, Jan. 2015, doi: 10.1016/j.talanta.2014.08.055.
31. M. Rani *et al.*, "Understanding the mechanism of replacement of citrate from the surface of gold nanoparticles by amino acids: A theoretical and experimental investigation and their biological application," *RSC Adv*, vol. 6, no. 21, pp. 17373–17383, 2016, doi: 10.1039/c5ra26502a.
32. R. Ranjan, M. A. Kirillova, and V. A. Kratasyuk, "Ethylene diamine functionalized citrate-capped gold nanoparticles for metal-enhanced bioluminescence," *Journal of Siberian Federal University - Biology*, vol. 13, no. 3, pp. 322–330, 2020, doi: 10.17516/1997-1389-0330.
33. B. Contreras-Trigo *et al.*, "Slight ph fluctuations in the gold nanoparticle synthesis process influence the performance of the citrate reduction method," *Sensors (Switzerland)*, vol. 18, no. 7, Jul. 2018, doi: 10.3390/s18072246.
34. P. Wulandari, T. Nagahiro, N. Fukada, Y. Kimura, M. Niwano, and K. Tamada, "Characterization of citrates on gold and silver nanoparticles," *J Colloid Interface Sci*, vol. 438, pp. 244–248, Jan. 2015, doi: 10.1016/j.jcis.2014.09.078.
35. B. R. Khalkho *et al.*, "Citrate functionalized gold nanoparticles assisted micro extraction of L-cysteine in milk and water samples using Fourier transform infrared spectroscopy," *Spectrochim Acta A Mol Biomol Spectrosc*, vol. 267, Feb. 2022, doi: 10.1016/j.saa.2021.120523.
36. M. S. Frost, M. J. Dempsey, and D. E. Whitehead, "The response of citrate functionalised gold and silver nanoparticles to the addition of heavy metal ions," *Colloids and Surfaces A: Physicochemical and Engineering Aspects*, vol. 518. Elsevier B.V., pp. 15–24, Apr. 05, 2017. doi: 10.1016/j.colsurfa.2016.12.036.
37. I. Y. Elbeyli, "Production of crystalline boric acid and sodium citrate from borax decahydrate," *Hydrometallurgy*, vol. 158, pp. 19–26, Dec. 2015, doi: 10.1016/J.HYDROMET.2015.09.022.
38. J. Gao, Y. Wang, and H. Hao, "Investigations on dehydration processes of trisodium citrate hydrates," *Front Chem Sci Eng*, vol. 6, no. 3, pp. 276–281, Sep. 2012, doi: 10.1007/S11705-012-1206-4/METRICS.
39. G. Rajakumar *et al.*, "Biosynthesis and biomedical applications of gold nanoparticles using eclipta prostrata leaf extract," *Applied Sciences (Switzerland)*, vol. 6, no. 8, Aug. 2016, doi: 10.3390/app6080222.
40. B. Sadeghi, M. Mohammadzadeh, and B. Babakhani, "Green synthesis of gold nanoparticles using Stevia rebaudiana leaf extracts: Characterization and their stability," *J Photochem Photobiol B*, vol. 148, pp. 101–106, Jul. 2015, doi: 10.1016/J.JPHOTOBIOL.2015.03.025.
41. C. R. Badita, D. Aranghel, C. Burducea, and P. Mereuta, "CHARACTERIZATION OF SODIUM ALGINATE BASED FILMS," 2020.

42. S. Liu, Y. Li, and L. Li, "Enhanced stability and mechanical strength of sodium alginate composite films," *Carbohydr Polym*, vol. 160, pp. 62–70, Mar. 2017, doi: 10.1016/j.carbpol.2016.12.048.
43. N. U. Islam, R. Amin, M. Shahid, and M. Amin, "Gummy gold and silver nanoparticles of apricot (Prunus armeniaca) confer high stability and biological activity," *Arabian Journal of Chemistry*, vol. 12, no. 8, pp. 3977–3992, Dec. 2019, doi: 10.1016/j.arabjc.2016.02.017.
44. T. C. Ho, M. H. Kim, Y.-J. Cho, J.-S. Park, S. Y. Nam, and B.-S. Chun, "Gelatin-sodium alginate based films with Pseuderanthemum palatiferum (Nees) Radlk. freeze-dried powder obtained by subcritical water extraction," *Food Packag Shelf Life*, vol. 24, p. 100469, 2020.
45. A. F. Martins *et al.*, "Preparation and cytotoxicity of N,N,N-trimethyl chitosan/alginate beads containing gold nanoparticles," *Int J Biol Macromol*, vol. 72, pp. 466–471, Jan. 2015, doi: 10.1016/j.ijbiomac.2014.08.020.
46. A. Ahmad *et al.*, "A critical review on the synthesis of natural sodium alginate based composite materials: An innovative biological polymer for biomedical delivery applications," *Processes*, vol. 9, no. 1. MDPI AG, pp. 1–27, Jan. 01, 2021. doi: 10.3390/pr9010137.
47. R. Ghorbani-Vaghei, H. Veisi, M. H. Aliani, P. Mohammadi, and B. Karmakar, "Alginate modified magnetic nanoparticles to immobilization of gold nanoparticles as an efficient magnetic nanocatalyst for reduction of 4-nitrophenol in water," *J Mol Liq*, vol. 327, Apr. 2021, doi: 10.1016/j.molliq.2020.114868.
48. J. Chen *et al.*, "Characterization of sodium alginate-based films incorporated with thymol for fresh-cut apple packaging," *Food Control*, vol. 126, Aug. 2021, doi: 10.1016/j.foodcont.2021.108063.
49. S. Liu, Y. Li, and L. Li, "Enhanced stability and mechanical strength of sodium alginate composite films," *Carbohydr Polym*, vol. 160, pp. 62–70, Mar. 2017, doi: 10.1016/J.CARBPOL.2016.12.048.
50. R. K. Ramakrishnan, S. Wacławek, M. Černík, and V. V. T. Padil, "Biomacromolecule assembly based on gum kondagogu-sodium alginate composites and their expediency in flexible packaging films," *Int J Biol Macromol*, vol. 177, pp. 526–534, Apr. 2021, doi: 10.1016/J.IJBIOMAC.2021.02.156.
51. M. Moosavi-Nasab, S. Khoshnoudi-Nia, Z. Azimifar, and S. Kamyab, "Evaluation of the total volatile basic nitrogen (TVB-N) content in fish fillets using hyperspectral imaging coupled with deep learning neural network and meta-analysis," *Sci Rep*, vol. 11, no. 1, Dec. 2021, doi: 10.1038/s41598-021-84659-y.
52. A. Rizo, V. Mañes, A. Fuentes, I. Fernández-Segovia, and J. M. Barat, "Physicochemical and microbial changes during storage of smoke-flavoured salmon obtained by a new method," *Food Control*, vol. 56, pp. 195–201, Oct. 2015, doi: 10.1016/j.foodcont.2015.03.030.
53. S. Wang, W. Xiang, H. Fan, J. Xie, and Y. F. Qian, "Study on the mobility of water and its correlation with the spoilage process of salmon (Salmo solar) stored at 0 and 4 °C by low-field nuclear magnetic resonance (LF NMR 1H)," *J Food Sci Technol*, vol. 55, no. 1, pp. 173–182, Jan. 2018, doi: 10.1007/s13197-017-2880-5.
54. Z. Jia, C. Shi, Y. Wang, X. Yang, J. Zhang, and Z. Ji, "Nondestructive determination of salmon fillet freshness during storage at different temperatures by electronic nose system combined with radial basis function neural networks," *Int J Food Sci Technol*, vol. 55, no. 5, pp. 2080–2091, May 2020, doi: 10.1111/ijfs.14451.
55. J. Xie, Z. Zhang, S. P. Yang, Y. Cheng, and Y. F. Qian, "Study on the spoilage potential of Pseudomonas fluorescens on salmon stored at different temperatures," *J Food Sci Technol*, vol. 55, no. 1, pp. 217–225, Jan. 2018, doi: 10.1007/s13197-017-2916-x.
56. M. Mikš-Krajnik, Y. J. Yoon, D. O. Ukuku, and H. G. Yuk, "Volatile chemical spoilage indexes of raw Atlantic salmon (Salmo salar) stored under aerobic condition in relation to microbiological and sensory shelf lives," *Food Microbiol*, vol. 53, pp. 182–191, Feb. 2016, doi: 10.1016/j.fm.2015.10.001.
57. J. H. Cheng and D. W. Sun, "Recent Applications of Spectroscopic and Hyperspectral Imaging Techniques with Chemometric Analysis for Rapid Inspection of Microbial Spoilage in Muscle Foods," *Compr Rev Food Sci Food Saf*, vol. 14, no. 4, pp. 478–490, Jul. 2015, doi: 10.1111/1541-4337.12141.
58. H. I. Hsiao and J. N. Chang, "Developing a microbial time–temperature indicator to monitor total volatile basic nitrogen change in chilled vacuum-packed grouper fillets," *J Food Process Preserv*, vol. 41, no. 5, Oct. 2017, doi: 10.1111/jfpp.13158.
59. N. Wiernasz, J. Cornet, M. Cardinal, M. F. Pilet, D. Passerini, and F. Leroi, "Lactic acid bacteria selection for biopreservation as a part of hurdle technology approach applied on seafood," *Front Mar Sci*, vol. 4, no. MAY, May 2017, doi: 10.3389/fmars.2017.00119.
60. N. Abel, B. T. Rotabakk, T. Rustad, V. B. Ahlsen, and J. Lerfall, "Physiochemical and Microbiological Quality of Lightly Processed Salmon (Salmo salar L.) Stored Under Modified Atmosphere," *J Food Sci*, vol. 84, no. 12, pp. 3364–3372, Dec. 2019, doi: 10.1111/1750-3841.14852.